Title	Nickel Carbide Nanoparticle Catalyst for Selective Hydrogenation of Nitriles to Primary Amines
Author(s)	Yamaguchi, Sho; Kiyohira, Daiki; Tada, Kohei et al.
Citation	Chemistry - A European Journal. 2024, 30(13), p. e202303573
Version Type	VoR
URL	https://hdl.handle.net/11094/95263
rights	This article is licensed under a Creative Commons Attribution-NonCommercial 4.0 International License.
Note	

Nickel Carbide Nanoparticle Catalyst for Selective Hydrogenation of Nitriles to Primary Amines

Sho Yamaguchi,[a, b] Daiki Kiyohira,[a] Kohei Tada,[c] Taiki Kawakami,[a] Akira Miura,[d, e] Takato Mitsudome,[a, b, e] and Tomoo Mizugaki*[a, b, f]

Despite its unique physicochemical properties, the catalytic application of nickel carbide (Ni_3C) in organic synthesis is rare. In this study, we report well-defined nanocrystalline Ni_3C (nano-Ni_3C) as a highly active catalyst for the selective hydrogenation of nitriles to primary amines. The activity of the aluminum-oxide-supported nano-Ni_3C (nano-Ni_3C/Al_2O_3) catalyst surpasses that of Ni nanoparticles. Various aromatic and aliphatic nitriles and dinitriles were successfully converted to the corresponding primary amines under mild conditions (1 bar H_2 pressure). Furthermore, the nano-Ni_3C/Al_2O_3 catalyst was reusable and applicable to gram-scale experiments. Density functional theory calculations suggest the formation of polar hydrogen species on the nano-Ni_3C surface, which were attributed to the high activity of nano-Ni_3C towards nitrile hydrogenation. This study demonstrates the utility of metal carbides as a new class of catalysts for liquid-phase organic reactions.

Introduction

Metal carbides possess several unique properties, including high electrical conductivity, mechanical strength and hardness, and high stability,[1,2] which have attracted considerable atten-

[a] Dr. S. Yamaguchi, D. Kiyohira, T. Kawakami, Dr. T. Mitsudome, Prof. Dr. T. Mizugaki
Department of Materials Engineering Science, Graduate School of Engineering Science
Osaka University
1-3 Machikaneyama, Toyonaka, Osaka 560-8531, Japan
E-mail: mizugaki.tomoo.es@osaka-u.ac.jp

[b] Dr. S. Yamaguchi, Dr. T. Mitsudome, Prof. Dr. T. Mizugaki
Innovative Catalysis Science Division, Institute for Open and Transdisciplinary Research Initiatives (ICS-OTRI)
Osaka University
Suita, Osaka 565-0871, Japan

[c] Dr. K. Tada
Research Institute of Electrochemical Energy (RIECEN), Department of Energy and Environment
National Institute of Advanced Industrial Science and Technology (AIST)
1-8-31 Midorigaoka, Ikeda, Osaka 563-8577, Japan

[d] Dr. A. Miura
Division of Applied Chemistry, Faculty of Engineering
Hokkaido University
Kita 13, Nishi 8, Sapporo, Hokkaido 060-8628, Japan

[e] Dr. A. Miura, Dr. T. Mitsudome
PRESTO, Japan Science and Technology Agency (JST)
4-1-8 Honcho, Kawaguchi, Saitama 333-0012, Japan

[f] Prof. Dr. T. Mizugaki
Research Center for Solar Energy Chemistry, Graduate School of Engineering Science
Osaka University
1-3 Machikaneyama, Toyonaka, Osaka 560-8531, Japan

Supporting information for this article is available on the WWW under https://doi.org/10.1002/chem.202303573

tion across various fields, such as superconducting materials[3] and solar heat absorbers.[4] Recent advancements in nanotechnology have enabled the precise synthesis of metal carbide nanoparticles (NPs), opening avenues for their catalytic functions to be explored.[5] In particular, nickel carbide NPs (Ni_3C NPs) have shown great potential as electrodes in O_2/H_2 evolution reactions,[6–9] photocatalytic applications,[10] and dry reforming of methane.[11] However, despite their unique catalytic properties, the application of Ni_3C NPs in liquid-phase molecular transformations is rare.[12] Therefore, investigating the potential of Ni_3C NP catalysts in the liquid-phase is of great interest in organic synthesis.

The hydrogenation of nitriles into primary amines plays a pivotal role in the production of solvents, surfactants, and numerous essential building blocks in fine chemical synthesis. Noble metal catalysts, such as Ru[13,14] and Pd,[15,16] are among the most effective heterogeneous catalysts for nitrile hydrogenation. Nevertheless, the scarcity and high cost of noble metals impede their widespread industrial use. Alternatively, non-noble metal catalysts are widely used in the industrial hydrogenation of nitriles owing to their earth-abundance and low-cost.[17] However, metallic catalysts like Ni,[18–28] Co,[29–32] and Fe[33] typically require harsh reaction conditions, including high temperatures and H_2 pressures. Consequently, developing non-noble-metal catalysts that exhibit high activity under mild conditions is of great importance.[34–37]

In this study, we synthesized well-defined nanocrystalline Ni_3C (nano-Ni_3C), and its catalytic performance was evaluated. It was found that nano-Ni_3C supported on aluminum oxide (nano-Ni_3C/Al_2O_3) exhibited high catalytic activity in the hydrogenation of nitriles to primary amines, even under atmospheric H_2 pressure. The catalytic performance of nano-Ni_3C/Al_2O_3 significantly differed from that of Ni NPs. nano-Ni_3C/Al_2O_3 displayed a broad substrate scope and good reusability. We performed density functional theory (DFT) calculations to explain the high catalytic performance of nano-Ni_3C.

Chem. Eur. J. **2024**, *30*, e202303573 (1 of 7)

© 2024 The Authors. Chemistry - A European Journal published by Wiley-VCH GmbH

Chemistry–A European Journal

Research Article
doi.org/10.1002/chem.202303573

Chemistry
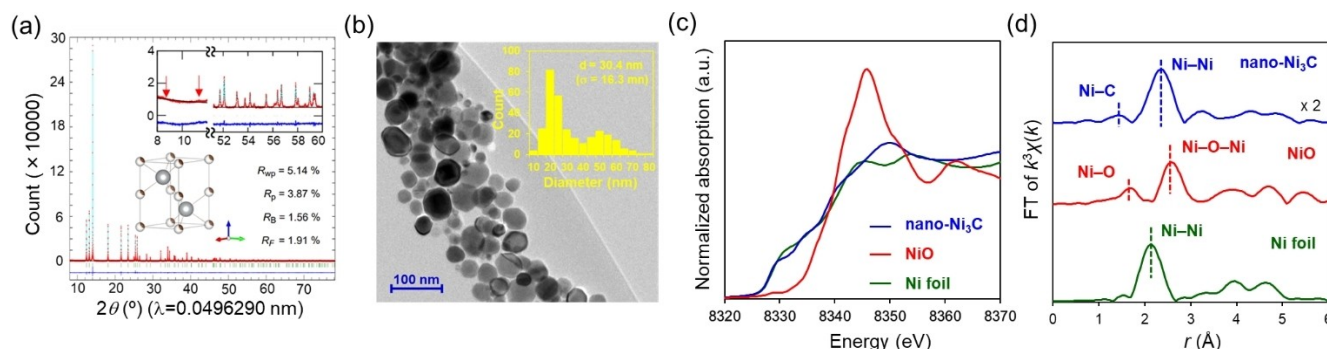Europe
European Chemical
Societies Publishing

Figure 1. Structural and morphological characterization of nano-Ni₃C. (a) Rietveld refinement profile of synchrotron XRD spectrum and structural model. Observed (red), calculated (sky-blue) patterns, and the difference (blue) between them resulting from Rietveld analysis. Green vertical bars denote positions of Bragg diffraction. Red arrows in the inset indicate the absence of superstructure peaks. (b) TEM image with size distribution histogram (inset). (c) Ni *K*-edge XANES spectra and (d) Ni *K*-edge FT-EXAFS spectra of nano-Ni₃C, NiO, and Ni foil.

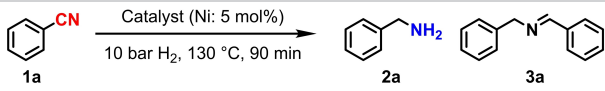## Results and Discussion

Characterization of nano-Ni₃C

Figure 1a presents the Rietveld analysis of nano-Ni₃C (Tables S1 and S2). Ni₃C is a non-stoichiometric compound that is known to adopt two different hexagonal structures: one with hexagonal parameters of $a = 2.6449$ Å and $c = 4.3296$ Å[38] and the other as a superstructure with the lattice parameters of $a = 4.555$ Å and $c = 12.92$ Å where the *a*- and *c*-axis is approximately square root of three times longer and three times longer, respectively.[39] The absence of superlattice peaks at lower angles, indicated by red arrows, and the improved fitting factor, R_{wp}, transitioning from 5.54% (superstructure) to 5.14% (simple structure) suggest a simple structure, with $a = 0.264965(1)$ nm and $c = 0.433573(1)$ nm. The occupation of the C site converged to 0.309(3); thus, the chemical formula was Ni₃C₀.₉₂₇₍₉₎. Furthermore, a representative transmission electron microscopy (TEM) image of nano-Ni₃C illustrates the formation of spherical particles with sizes ranging from 10–80 nm (Figure 1b). The electronic states of the Ni species in nano-Ni₃C were identified using X-ray absorption fine structure (XAFS) spectroscopy. The absorption edge energy in the Ni *K*-edge X-ray absorption near edge structure (XANES) spectrum of nano-Ni₃C closely resembled that of Ni foil, indicating that Ni species in nano-Ni₃C existed in a metallic state (Figure 1c). This result is in good agreement with the X-ray photoelectron spectra, where two peaks at 852.9 and 870.1 eV in the spectrum of nano-Ni₃C are similar to those of Ni $2_{p3/2}$ (852.7 eV) and Ni $2_{p1/2}$ (870.0 eV),[40] respectively, in the spectrum of metallic Ni (Figure S1). Figure 1d displays the Fourier transform of the extended XAFS (FT-EXAFS) spectrum of nano-Ni₃C, with NiO and Ni foils as references. The peaks at 1.50 and 2.42 Å in the spectrum of nano-Ni₃C were assigned to the Ni–C and Ni–Ni shells, respectively. The curve-fitting analyses of the EXAFS spectra are shown in Figure S2 and the results are summarized in Table S3. The Ni–Ni bond is longer than that in the Ni foil owing to the expansion of the Ni lattice resulting from the insertion of carbon atoms. Moreover, the absence of Ni–O bonds indicates that the nano-Ni₃C was not oxidized, which is consistent with

the XANES and X-ray photoelectron spectra. These results clearly demonstrate the successful synthesis of spherical, phase-pure nano-Ni₃C.

### Catalytic Performance of nano-Ni₃C in the Hydrogenation of Nitriles

Using ammonia as additives is crucial to promote the selective hydrogenation of **1a** to primary amines (see Scheme S1).[41] Thus, the hydrogenation of **1a** using nano-Ni₃C was performed in the presence of NH₃ aq. at 130°C under 10 bar H₂ to afford benzylamine (**2a**) and *N*-benzylidenebenzylamine (**3a**) in 31% and 8% yields, respectively (Table 1, Entry 1). nano-Ni₃C can be easily immobilized on various support materials. nano-Ni₃C/Al₂O₃ demonstrated high activity, yielding **2a** in a 68% yield (Table 1, Entry 2). The performance of nano-Ni₃C/Al₂O₃ surpassed those of nano-Ni₃C on other supports of hydrotalcite (HT), TiO₂, SiO₂, and activated carbon (see Scheme S2, Figures S3, and Tables S4,5). By increasing the amount of nano-Ni₃C/Al₂O₃, **2a** was obtained in >99% yield (Table 1, Entry 4). These results revealed that the combination of nano-Ni₃C and γ-Al₂O₃

Table 1. Hydrogenation of benzonitrile (**1a**) to benzylamine (**2a**) using various Ni catalysts.[a]

Entry	Catalyst	Conv. of **1a** [%][b]	Yield of **2a** [%][b]	Yield of **3a** [%][b]
1	nano-Ni₃C	45	31	8
2	nano-Ni₃C/Al₂O₃	78	68	9
3	Ni NPs/Al₂O₃	29	16	7
4[c]	nano-Ni₃C/Al₂O₃	>99	>99	<1

[a] Reaction conditions: **1a** (0.5 mmol), 2-propanol (3 mL), and 25% NH₃ aq. (1.2 mL). [b] Conversion and yields were determined by gas chromatography-flame ionization detection (GC-FID) using an internal standard method. [c] Ni 10 mol%.

provided superior catalytic performance for nitrile hydrogenation. The differences in the catalytic activities of the nano-Ni_3C and Ni NPs were investigated using Ni NPs prepared with a similar shape and size to those of nano-Ni_3C (Figures S4–S6, see Experimental section for details). In the hydrogenation of **1a**, Ni NPs/Al_2O_3 afforded **2a** in 16% yield (Table 1, Entry 3). The yield of **2a** obtained using nano-Ni_3C/Al_2O_3 was four times higher than that obtained using Ni NPs/Al_2O_3 (Table 1, Entries 2 and 3), clearly demonstrating the outstanding activity of the nano-Ni_3C/Al_2O_3 catalyst.
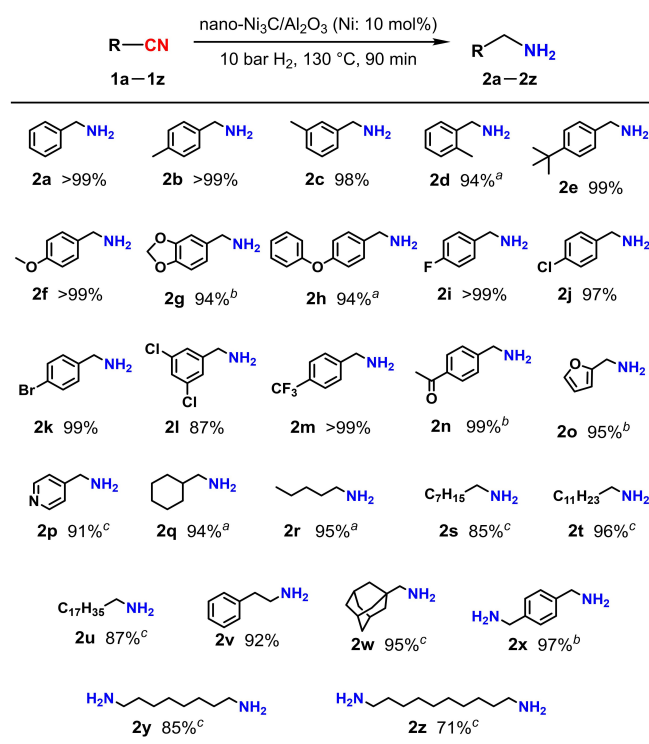
Scheme 1. Hydrogenation of various nitriles using the nano-Ni_3C/Al_2O_3 catalyst. Reaction conditions: nano-Ni_3C/Al_2O_3 (0.058 g), substrate (0.5 mmol), 2-propanol (3 mL), 25% NH_3 aq. (1.2 mL). Yields were determined by gas chromatography-mass spectrometry (GC-MS) using an internal standard method. [a] 40 bar H_2, 6 h. [b] 3 h. [c] 150 °C, 40 bar H_2, 12 h.

Applicability and Durability of nano-Ni_3C in Nitrile Hydrogenation

To demonstrate the broad applicability of nano-Ni_3C/Al_2O_3, the substrate scope was investigated using various (hetero)aromatic and aliphatic nitriles (Scheme 1). Benzonitriles with electron-donating (—Me, —tBu, —OMe, and —OPh) and electron-withdrawing groups (—F, —Cl, —Br, —CF_3 and —acetyl) were efficiently hydrogenated to the corresponding primary amines **2a–2n** in high yields. The nano-Ni_3C/Al_2O_3 catalyst showed high chemoselectivity toward nitrile group in the intramolecular competitive reaction of halogen substituted benzonitrile; the Cl— and Br— groups of aromatic nitriles (**1j**, **1k**) remained intact under the examined reaction conditions, although the supported Ni catalysts are known to promote the hydrodehalogenation of aryl halides.[42,43] Indeed, hydrogenation of **1j** using Ni NPs/Al_2O_3 catalyst afforded **2j** with the dehalogenated product **2b**, clearly demonstrating the advantages of the nano-Ni_3C/Al_2O_3 catalyst enabling the chemoselective hydrogenation of halo-benzonitriles (Table S6). 4-Iodobenzonitrile resulted in low selectivity to desired primary amine (Scheme S3a). 4-Aminobenzonitrile was not reacted at all (Scheme S3b). The heteroaromatic nitriles 2-furancarbonitrile (**1o**) and 4-cyanopyridine (**1p**) were converted into the desired amines **2o** and **2p**, respectively, in excellent yields; however, hydrogenation of 2-thiophenecarbonitrile did not proceed (Scheme S3c). The aliphatic nitriles **1q–1v** were also converted to the corresponding amines in high yields, and the sterically hindered nitrile **1w** smoothly underwent hydrogenation to produce amine **2w** in 95% yield. Furthermore, the hydrogenation of the aromatic and aliphatic dinitriles **1x**, **1y**, and **1z** afforded the corresponding diamines **2x**, **2y**, and **2z**, which are important precursors in the synthesis of valuable plastics and fibers, in satisfactory yields. These results clearly demonstrate the versatility and substrate scope of nano-Ni_3C/Al_2O_3 in the hydrogenation of nitriles to primary amines.

In contrast to most existing non-noble metal catalysts, which require high-pressure H_2, this nano-Ni_3C catalyst system operates well under atmospheric H_2 pressure (Tables 2 and S7); nano-Ni_3C/Al_2O_3 efficiently hydrogenated a wide range of aromatic and aliphatic nitriles into the corresponding primary

Table 2. Comparison of activity between nano-Ni_3C and reported Ni catalysts for hydrogenation of **1a**.

| Catalyst	Reaction conditions	Yield of **2a** [%]	TON[a]	Ref.
nano-Ni_3C/Al_2O_3	10 mol% Ni, 2-propanol, NH_3 aq., 10 bar H_2, 130 °C, 90 min.	99	10	**This work** (Table 1 entry 4)
nano-Ni_3C/Al_2O_3	10 mol% Ni, 2-propanol, NH_3 aq., 1 bar H_2, 150 °C, 14 h.	99	10	**This work** (Scheme 2)
nano-Ni_3C/Al_2O_3	0.1 mol% Ni, 2-propanol, NH_3 aq., 45 bar H_2, 150 °C, 40 h.	90	900	**This work** (Scheme 3)
nano-Ni_2P	5 mol% Ni, NH_3 aq., 40 bar H_2, 130 °C, 3 h.	95	19	35
nano-Ni_2P	5 mol% Ni, NH_3 aq., 1 bar H_2, 150 °C, 12 h.	85	17	35
Ni NPs[b]	0.7 mol% Ni, [BMIM]NTf₂, 25 bar H_2, 90 °C, 22 h.	80	114	21
Ni-phen@SiO_2	4.5 mol% Ni, 7 M NH_3/MeOH, 50 bar H_2, 100 °C, 20 h.	91	20	23
MC/Ni	13 mol% Ni, MeOH, NH_3 aq. (36 wt. %), 2.5 bar H_2, 80 °C, 6 h.	>99	8	25
$NiMg_{0.75}Al_{0.25}O$-op	12 mol% Ni, MeOH, 40 bar H_2, 100 °C, 2 h.	91	8	26
Ni/Al_2O_3-600	12 mol% Ni, EtOH, NH_3·H_2O (36.5 wt%), 2.5 bar H_2, 60 °C, 6 h.	95	8	27

[a] Based on total active metal atoms. [b] Embedded in imidazolium based ionic liquids.

amines (**2a**, **2b**, **2f**, **2i**–**2k**, **2m**, **2n**, **2r** and **2v**, Scheme 2). The nano-Ni$_3$C/Al$_2$O$_3$ catalyst also enabled gram-scale hydrogenation. Under organic solvent-free conditions, 2.1 g of **1a** was efficiently converted to **2a**, which was obtained as the hydrochloride salt in 90% isolated yield with a turnover number of 900. This turnover number is among the highest reported in nitrile hydrogenation (Scheme 3a and Tables 2 and S7). Hydrogenation of the dinitrile 1,4-dicyanobenzene (**1x**) afforded the diamine product in 79% isolated yield (Scheme 3b).

A hot filtration experiment was performed to confirm that the hydrogenation of nitriles proceeded on the nano-Ni$_3$C/Al$_2$O$_3$
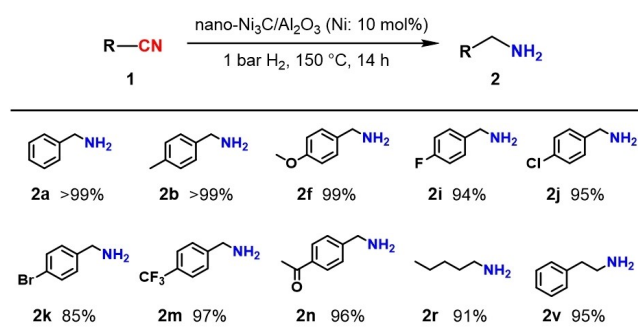
Scheme 2. Hydrogenation of various nitriles using the nano-Ni$_3$C/Al$_2$O$_3$ catalyst under 1 bar H$_2$. Reaction conditions: nano-Ni$_3$C/Al$_2$O$_3$ (0.058 g), substrate (0.5 mmol), 2-propanol (1.5 mL), 25% NH$_3$ aq. (0.6 mL).
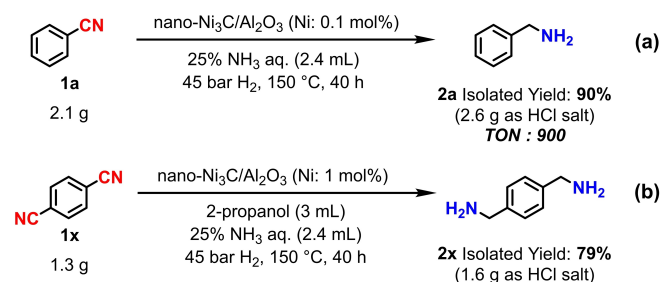
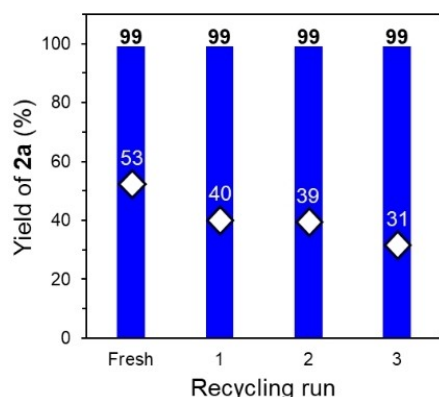**Scheme 3.** Gram-scale hydrogenation of (a) **1a** and (b) **1x** with nano-Ni$_3$C/Al$_2$O$_3$.

Figure 2. Evaluation of the nano-Ni$_3$C/Al$_2$O$_3$-catalyzed hydrogenation of **1a** over 4 catalytic cycles. Reaction conditions: **1a** (0.5 mmol), nano-Ni$_3$C/Al$_2$O$_3$ (0.058 g, 10 mol% Ni), 2-propanol (3 mL), 25% NH$_3$ aq. (1.2 mL), H$_2$ (10 bar), 130 °C, blue bars and white diamonds represent reaction times of 90 min and 40 min, respectively.

surface (Figure S7). After the removal of the nano-Ni$_3$C/Al$_2$O$_3$ catalyst from a reaction mixture that provided a 53% yield of **2a**, the filtrate was treated under the optimized reaction conditions (Table 1); consequently, no additional **2a** was detected in the filtrate. Moreover, the nano-Ni$_3$C/Al$_2$O$_3$ catalyst was easily separated from the reaction mixture and reused without pre-treatment. After four reactions, there was no reduction in the yield of **2a** (Figure 2). To obtain more detailed information regarding the catalyst reusability, the initial rate was further investigated during the recycling experiments at an incomplete reaction time (40 min). A reduction in the yield of **2a** was observed (diamonds in Figure 2). The powder X-ray diffraction (XRD) patterns (Figure S8) of nano-Ni$_3$C/Al$_2$O$_3$ obtained before and after the reaction were identical. The Ni K-edge XANES spectrum and the result of the curve-fitting analysis of the EXAFS of the spent nano-Ni$_3$C/Al$_2$O$_3$ are very similar to those of the fresh nano-Ni$_3$C/Al$_2$O$_3$ (Figures S2,S9 and Table S3), indicating that the electronic state and the local structure of nano-Ni$_3$C/Al$_2$O$_3$ do not significantly change after the reaction. However, inductively coupled plasma atomic emission spectroscopy analyses showed that the amount of Ni in the spent catalyst was 0.7 wt% lower than that of the fresh sample (Table S8). The TEM image of the spent nano-Ni$_3$C/Al$_2$O$_3$ catalyst revealed that the average size of the Ni carbide NPs was slightly larger than those in the fresh catalyst (Figure 3), which would explain a slight reduction in the yield of **2a** during the reuse experiments.

Elucidation of the High Catalytic Performance of nano-Ni$_3$C/Al$_2$O$_3$

To elucidate the origin of the high catalytic activity of nano-Ni$_3$C/Al$_2$O$_3$, the influence of H$_2$ pressure and concentration of **1a** on the conversion rate was examined using nano-Ni$_3$C/Al$_2$O$_3$ and Ni NPs/Al$_2$O$_3$ catalysts (Figure 4). In these experiments, the ranges of H$_2$ pressure and **1a** amount are 10–40 bars and 0.4–1.2 mmol, respectively (Figure S10). The initial rates using nano-Ni$_3$C/Al$_2$O$_3$ showed no correlation with H$_2$ pressure, but were positively correlated with the concentration of **1a**. Conversely, the initial reaction rates using Ni NPs/Al$_2$O$_3$ were dependent on the H$_2$ pressure and were independent of the concentration of **1a**. Previous reports on the nitrile hydrogenation using Ni NPs revealed that the initial rates were more strongly dependent on the H$_2$ pressure than on the substrate concentration, which are
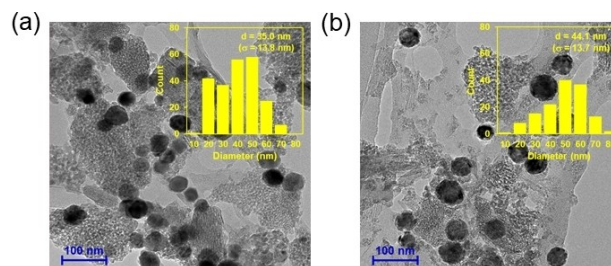

Figure 3. TEM images of (a) fresh and (b) spent nano-Ni$_3$C/Al$_2$O$_3$.

Chemistry–A European Journal

Research Article
doi.org/10.1002/chem.202303573

Chemistry Europe
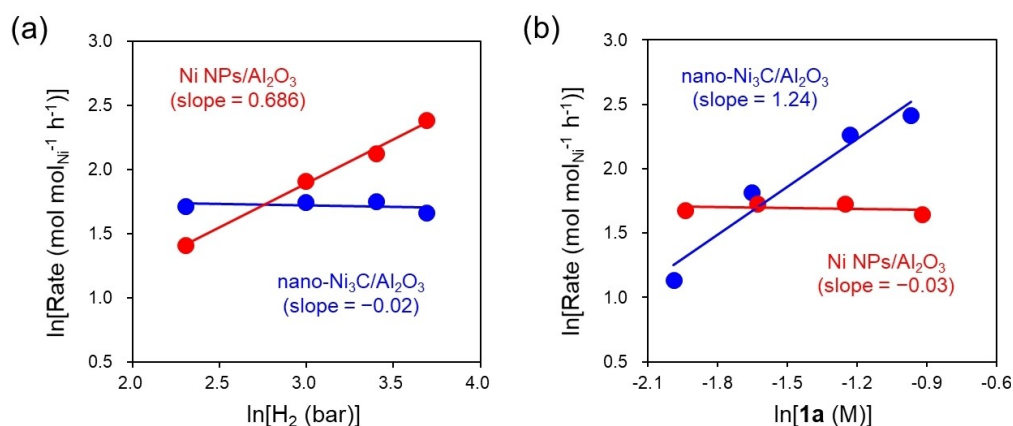European Chemical
Societies Publishing

Figure 4. Dependence of the initial reaction rate on (a) H₂ pressure and (b) concentration of **1 a**. Reaction conditions: **1 a** (0.4–1.2 mmol), nano-Ni₃C/Al₂O₃ (4.0–12.5 mol%), 2-propanol (3 mL), 25 % NH₃ aq. (1.2 mL), H₂ (10–40 bar), 130 °C, 10–35 min.

consistent with the above results.[44–46] These results indicate that H₂ strongly interacts with nano-Ni₃C/Al₂O₃ under the examined nitrile hydrogenation conditions.

DFT calculations were performed to gain additional insight into the interaction between H₂ and the nano-Ni₃C surface (**Supporting Information**). Based on previous reports,[47,48] the present study adopted a C-terminated (C-rich Ni₃C(113)) model surface (Figure S12). The adsorption of H by C-rich Ni₃C(113) occurs at tri-coordinate C exposed on the model surface; adsorption onto the on-top site is the most stable, with an adsorption energy (E_{ad}) of -1.01 eV (Figure 5a). Figures 5b–5d show the adsorption of H on the hexagonal close-packed (hcp), face-centered cubic (fcc), and body-centered cubic (bcc) hollow sites of Ni, respectively. The E_{ad} values of the hollow sites range from 0.5–0.7 eV, and these adsorptions were 0.3–0.5 eV less stable than the most stable adsorption ($E_{ad} = -1.01$ eV). Conversely, the E_{ad} of H adsorption on the fcc hollow site of the Ni(111) surface was -0.57 eV (Figure 5e). H adsorption readily occurs on tri-coordinate C and at hollow Ni sites of the C-rich

Ni₃C(113) surface, indicating that the dissociated hydrogen species interact more strongly with nano-Ni₃C than with Ni NPs.

The properties of hydrogen species adsorbed on nano-Ni₃C surface were further discussed. The number of valence electrons of H (H_{ne}) adsorbed on the Ni hollow sites of Ni₃C(113) is greater than 1, that is they are hydridic, whereas the H adsorbed on the tri-coordinate C is slightly protonic (Figure 5). This suggests that H₂ strongly adsorbed on nano-Ni₃C surface is dissociated in a heterolytic manner. In contrast, H₂ is typically homolytically dissociated on the Ni NP surface.[49,50] In addition, hydrogen species formed through the heterolytic dissociation of H₂ are known to be more effective for nitrile hydrogenation than those formed through homolytic dissociation.[50–54] Hence, the high catalytic activity of nano-Ni₃C can be explained as follows: the hydridic H adsorbed on the Ni sites of nano-Ni₃C reacts with nitriles, whereupon the H adsorbed on the carbon atom is efficiently supplied to the substrate, thereby facilitating the hydrogenation of nitriles.
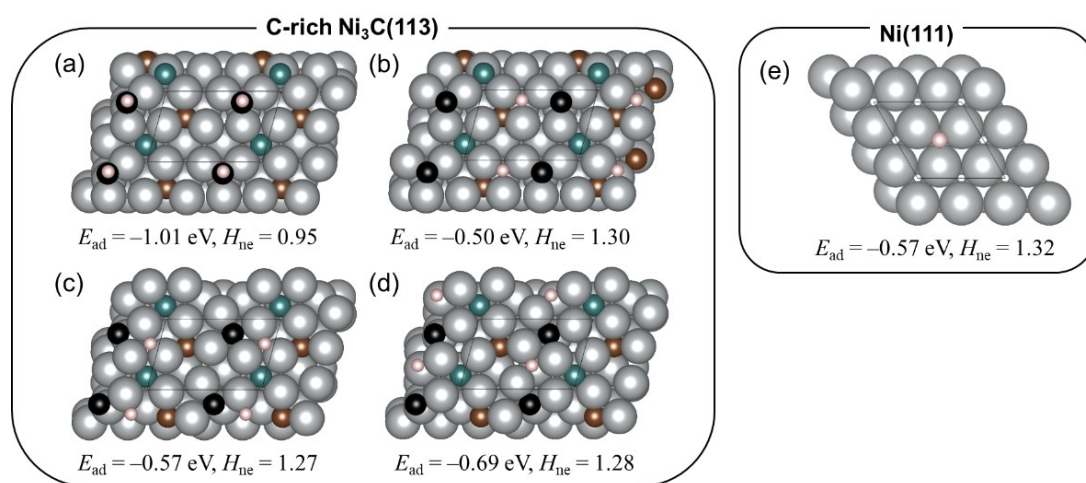

Figure 5. Top views of typical adsorption structures of H/Ni₃C(113) and H/Ni(111) with their E_{ad} and H_{ne} values estimated by DFT calculations. (a–d) C-rich Ni₃C(113) and (e) Ni(111). All initial and optimized structures are summarized in the **Supporting Information**. Black, green, and brown spheres represent tri-, penta-, and hexacoordinate C atoms before H adsorption, respectively. Gray and pale pink spheres represent Ni and H atoms, respectively.

Chemistry–A European Journal

Research Article
doi.org/10.1002/chem.202303573

Chemistry Europe
European Chemical
Societies Publishing

Conclusions

We have synthesized phase-pure Ni_3C NPs (nano-Ni_3C) and demonstrated that the nano-Ni_3C catalyzes selective hydrogenation of nitrile to primary amine. The catalytic activity of nano-Ni_3C/Al_2O_3 is superior to that of Ni NPs/Al_2O_3. Furthermore, nano-Ni_3C/Al_2O_3 shows broad substrate scope, allowing the conversion of various (hetero)aromatic and aliphatic nitriles into the corresponding primary amines, even under 1 bar of H_2. nano-Ni_3C/Al_2O_3 can also be easily recovered and successfully reused for three times. DFT calculations suggest that polar H species were formed on the nano-Ni_3C surface through the heterolytic dissociation of H_2. Hydridic H adsorbed on Ni reacts with nitriles, whereupon the H adsorbed on carbidic carbon combines with the resulting substrate, which could be attributed to the excellent catalytic activity of nano-Ni_3C. We envisage that the attractive catalytic properties of nickel carbide can be applied to various liquid-phase hydrogenation reactions.

Experimental Section

Synthesis of nano-Ni_3C

All reactions were conducted in an Ar atmosphere using standard Schlenk line techniques. In a typical reaction, a mixture of $Ni(acac)_2$ (1.0 mmol) and oleylamine (30 mmol) was stirred at 120°C for 1 h *in vacuo* in a Schlenk flask.[55] The reaction temperature was then increased to 320°C and maintained constant for 3 h with continuous stirring, resulting in the formation of a black colloidal solution. After cooling the mixture to 25°C, a black precipitate was collected by adding *n*-hexane to the solution. The obtained product was washed through repeated redispersion and precipitation cycles using a mixed solvent containing ethanol and *n*-hexane (ethanol : *n*-hexane = 1 : 1). Subsequently, the resulting powder was dried overnight at 120°C *in vacuo* and stored in air.

Preparation of the Al_2O_3-supported nano-Ni_3C and Ni NPs

nano-Ni_3C (0.04 g) was dispersed in *n*-hexane (30 mL) and stirred with γ-Al_2O_3 (0.7 g) for 5 h at 25°C. The resulting powder was then dried *in vacuo* overnight at 25°C to yield nano-Ni_3C/Al_2O_3 as a gray powder. This product was stored in air at 25°C and used for characterization and reaction experiments without any pretreatment. nano-Ni_3C/Al_2O_3 was treated with flowing H_2 at 350°C for 3 h to produce Ni NPs/Al_2O_3. Figures S4–S6 show the TEM image, XRD pattern, and Ni *K*-edge XANES spectrum of Ni NPs/Al_2O_3, respectively. The Ni NPs in Ni NPs/Al_2O_3 exhibited an average particle size of 39.0 nm, which is similar to that of nano-Ni_3C/Al_2O_3. Ni NPs/Al_2O_3 was used as a catalyst without exposure to air.

General Procedure for Nitrile Hydrogenation

In a typical procedure, **1a** (0.5 mmol), 2-propanol (3 mL), and NH_3 aq. (25%, 1.2 mL) were added to nano-Ni_3C/Al_2O_3 (0.029 g, Ni: 5 mol%) in a 50 mL stainless-steel autoclave equipped with a Teflon inner cylinder. The reaction mixture was vigorously stirred at 130°C under 10 bar H_2. The conversion and yield of the reaction were determined by GC-FID, using diethylene glycol dimethyl ether as an internal standard. Primary amines were subsequently isolated in the form of hydrochloride salts. The crude reaction mixture was filtered to remove the solid catalyst, and NH_3 was removed under vacuum.

The mixture was then added to a solution of hydrogen chloride (1.25 M in 1,4-dioxane, 0.5 mL total volume). Analytically pure hydrochloride salts of the primary amines were obtained as solids (further details are provided in the **Supporting Information**).

Conflict of Interests

The authors declare no conflict of interest.

Data Availability Statement

The data that support the findings of this study are available on request from the corresponding author. The data are not publicly available due to privacy or ethical restrictions.

[1] W. S. Williams, *Prog. Solid State Chem.* **1971**, *6*, 57–118.
[2] J. S. Lee, *Metal Carbides. In Encyclopedia of Catalysis, 2nd ed.; Horvath, I. T., Ed.; John Wiley & Sons: New York*, **2003**, 1–33.
[3] A. Simon, *Angew. Chem. Int. Ed. Engl.* **1997**, *36*, 1788–1806.
[4] L. Borchardt, C. Hoffmann, M. Oschatz, L. Mammitzsch, U. Petasch, M. Herrmann, S. Kaskel, *Chem. Soc. Rev.* **2012**, *41*, 5053–5067.
[5] A. M. Alexander, J. S. J. Hargreaves, *Chem. Soc. Rev.* **2010**, *39*, 4388–4401.
[6] X. Fan, Z. Peng, R. Ye, H. Zhou, X. Guo, *ACS Nano* **2015**, *9*, 7407–7418.
[7] H. Wang, Y. Cao, G. Zou, Q. Yi, J. Guo, L. Gao, *ACS Appl. Mater. Interfaces* **2017**, *9*, 60–64.
[8] H. Fan, H. Yu, Y. Zhang, Y. Zheng, Y. Luo, X. Dai, B. Li, Y. Zong, Q. Yan, *Angew. Chem. Int. Ed.* **2017**, *56*, 12566–12570.
[9] J. Hao, G. Zhang, Y. Zheng, W. Luo, C. Jin, R. Wang, Z. Wang, W. Zheng, *Electrochim. Acta* **2019**, *320*, 134631.
[10] H. Zhang, Z. Luo, Y. Liu, Y. Jiang, *Appl. Catal. B* **2020**, *277*, 119166.
[11] J. G. Roblero, F. Pola-Albores, M. A. Valenzuela, E. Rojas-García, E. Ríos-Valdovinos, G. Valverde-Aguilar, *Int. J. Hydrogen Energy* **2019**, *44*, 10473–10483.

Chemistry–A European Journal

Research Article
doi.org/10.1002/chem.202303573

Chemistry Europe
European Chemical
Societies Publishing

[12] R. F. André, L. Meyniel, S. Carenco, *Catal. Sci. Technol.* **2022**, *12*, 4572–4583.

[13] D. Addis, S. Enthaler, K. Junge, B. Wendt, M. Beller, *Tetrahedron Lett.* **2009**, *50*, 3654–3656.

[14] D. Bagal, B. Bhanage, *Adv. Synth. Catal.* **2015**, *357*, 883–900.

[15] L. Hegedus, T. Mathe, *Appl. Catal. A* **2005**, *296*, 209–215.

[16] M. Chatterjee, H. Kawanami, N. Sato, T. Ishizaka, T. Yokoyama, T. Suzuki, *Green Chem.* **2010**, *12*, 87–93.

[17] S. Nishimura, *Handbook of Heterogeneous Catalytic Hydrogenation for Organic Synthesis; Wiley-VCH: Weinheim*, **2001**.

[18] A. C. Cope, H. R. Nace, *Org. Synth.* **1949**, 29.

[19] F. Roessler, *Chimia* **2003**, *57*, 791–798.

[20] F. Chen, C. Topf, J. Radnik, C. Kreyenschulte, H. Lund, M. Schneider, A. E. Surkus, L. He, K. Junge, M. Beller, *J. Am. Chem. Soc.* **2016**, *138*, 8781–8788.

[21] H. Konnerth, M. H. G. Prechtl, *New J. Chem.* **2017**, *41*, 9594–9597.

[22] P. Ji, K. Manna, Z. Lin, X. Feng, A. Urban, Y. Song, W. Lin, *J. Am. Chem. Soc.* **2017**, *139*, 7004–7011.

[23] P. Ryabchuk, G. Agostini, M. Pohl, H. Lund, A. Agapova, H. Junge, K. Junge, M. Beller, *Sci. Adv.* **2018**, *4*, eaat0761.

[24] K. Murugesan, T. Senthamarai, M. Sohail, A. S. Alshammari, M. M. Pohl, M. Beller, R. V. Jagadeesh, *Chem. Sci.* **2018**, *9*, 8553–8560.

[25] Y. Zhang, H. Yang, Q. Chi, Z. Zhang, *ChemSusChem* **2019**, *12*, 1246–1255.

[26] Y. Cao, H. Zhang, J. Dong, Y. Ma, H. Sun, L. Niu, X. Lan, L. Cao, G. Bai, *J. Mol. Catal.* **2019**, *475*, 110452.

[27] J. Wang, Q. Tang, S. Jin, Y. Wang, Z. Yuan, Q. Chi, Z. Zhang, *New J. Chem.* **2020**, *44*, 549–555.

[28] D. Formenti, R. Mocci, H. Atia, S. Dastgir, M. Anwar, S. Bachmann, M. Scalone, K. Junge, M. Beller, *Chem. Eur. J.* **2020**, *26*, 15589–15595.

[29] P. Ji, K. Manna, Z. Lin, X. Feng, A. Urban, Y. Song, W. Lin, *J. Am. Chem. Soc.* **2017**, *139*, 7004–7011.

[30] K. Murugesan, T. Senthamarai, M. Sohail, A. S. Alshammari, M. M. Pohl, M. Beller, R. V. Jagadeesh, *Chem. Sci.* **2018**, *9*, 8553–8560.

[31] S. Zhang, Y.-N. Duan, Y. Qian, W. Tang, R. Zhang, J. Wen, X. Zhang, *ACS Catal.* **2021**, *11*, 13761–13767.

[32] K. Kato, D. Deng, Y. Kita, K. Kamata, M. Hara, *Catal. Sci. Technol.* **2022**, *12*, 5425–5434.

[33] V. G. Chandrashekhar, T. Senthamarai, R. G. Kadam, O. Malina, J. Kašlík, R. Zbořil, M. B. Gawande, R. V. Jagadeesh, M. Beller, *Nat. Catal.* **2022**, *5*, 20–29.

[34] T. Mitsudome, M. Sheng, A. Nakata, J. Yamasaki, T. Mizugaki, K. Jitsukawa, *Chem. Sci.* **2020**, *11*, 6682–6689.

[35] S. Fujita, S. Yamaguchi, J. Yamasaki, K. Nakajima, S. Yamazoe, T. Mizugaki, T. Mitsudome, *Chem. Eur. J.* **2021**, *27*, 4439–4446.

[36] M. Sheng, S. Yamaguchi, A. Nakata, S. Yamazoe, K. Nakajima, J. Yamasaki, T. Mizugaki, T. Mitsudome, *ACS Sustainable Chem. Eng.* **2021**, *9*, 11238–11246.

[37] T. Tsuda, M. Sheng, H. Ishikawa, S. Yamazoe, J. Yamazaki, M. Hirayama, S. Yamaguchi, T. Mizugaki, T. Mitsudome, *Nat. Commun.* **2023**, *14*, 5959.

[38] L. J. E. Hofer, E. M. Cohn, W. C. Peebles, *J. Phys. Chem.* **1950**, *54*, 1161–1169.

[39] S. Nakamura, *J. Phys. Soc. Jpn.* **1958**, *13*, 1005–1014.

[40] J. F. Moulder, W. F. Stickle, P. E. Sobol, K. D. Bomben, *Handbook of X-ray Photoelectron Spectroscopy, Perkin-Elmer Corporation Physical Electronics Division*.

[41] J. Krupka, J. Pasek, *Curr. Org. Chem.* **2012**, *16*, 988–1004.

[42] W. Wu, J. Xu, R. Ohnishi, *Appl. Catal. B* **2005**, *60*, 129–137.

[43] D. K. Leonard, P. Ryabchuk, M. Anwar, S. Dastgir, K. Junge, M. Beller, *ChemSusChem* **2022**, *15*, e202102315.

[44] F. Hochard, H. Jobic, J. Massardier, A. J. Renouprez, *J. Mol. Catal. A* **1995**, *95*, 165–172.

[45] J. Krupka, J. Pasek, *Curr. Org. Chem.* **2012**, *16*, 988–1004.

[46] D. J. Segobia, A. F. Trasarti, C. R. Apesteguía, *React. Chem. Eng.* **2021**, *6*, 2181–2190.

[47] K. He, J. Xie, Z.-Q. Liu, N. Li, X. Chen, J. Hu, X. Li, *J. Mater. Chem. A* **2018**, *6*, 13110–13122.

[48] F. Hu, J. Peng, W. Xie, N. Li, *RSC Adv.* **2022**, *12*, 869–873.

[49] K. Christmann, *Surf. Sci. Rep.* **1988**, *9*, 1–163.

[50] D. R. Aireddy, K. Ding, *ACS Catal.* **2022**, *12*, 4707–4723.

[51] T. Mitsudome, Y. Mikami, M. Matoba, T. Mizugaki, K. Jitsukawa, K. Kaneda, *Angew. Chem. Int. Ed.* **2012**, *51*, 136–139.

[52] T. Mitsudome, Y. Yamamoto, Z. Maeno, T. Mizugaki, K. Jitsukawa, K. Kaneda, *J. Am. Chem. Soc.* **2015**, *137*, 13452–13455.

[53] B. Wyvratt, J. R. Gaudet, D. B. Pardue, A. Marton, S. Rudic, E. A. Mader, T. R. Cundari, J. M. Mayer, L. T. Thompson, *ACS Catal.* **2016**, *6*, 5797–5806.

[54] Y. Lu, J. Wang, X. Feng, Y. Li, W. Zhang, Y. Yamamoto, B. Ming, *Nanoscale* **2022**, *14*, 9341–9348.

[55] Y. Goto, K. Taniguchi, T. Omata, S. Otsuka-Yao-Matsuo, N. Ohashi, S. Ueda, H. Yoshikawa, Y. Yamashita, H. Oohashi, K. Kobayashi, *Chem. Mater.* **2008**, *20*, 4156–4160.